ACS OMEGA

Open Access

http://pubs.acs.org/journal/acsodf

Article

Properties and Microstructure of an Interfacial Transition Zone Enhanced by Silica Fume in Concrete Prepared with Coal Gangue as an Aggregate

Xianchen Wang, Xianhai Li,* Yanxia Zhong, Hong Li, and Jie Wang

Cite This: *ACS Omega* 2024, 9, 1870−1880

Read Online

ACCESS | Metrics & More | Article Recommendations

ABSTRACT: The wide application of concrete prepared with coal gangue (CG) as an aggregate (CPCGA) is limited because of the low mechanical strength and strong water absorption capacity of CG. This paper used silica fume (SF) to improve the performance of the interfacial transition zone (ITZ) in CPCGA and revealed the enhancement mechanism. The results showed that the compressive strength of CPCGA prepared with cement replaced by a suitable amount of SF at the age of 28 days increased by more than 30%, and the flexural strength increased by over 20%. The SF could effectively reduce the porosity and micropore size in the ITZ of CPCGA, and the porosity of the ITZ in CPCGA added with 7.50% SF decreased by 44.22, 46.16, and 24.46% at distances from the aggregate surface of 10, 50, and 100 μm, respectively, compared with CPCGA without SF. Further research showed that $Ca(OH)_2$ (CH) generated in the cement hydration reaction reacted with a large amount of active SiO_2 in SF to restrain the formation of coarse CH in the ITZ of CPCGA, and the calcium silicate hydrate (C−S−H) gel generated filled the ITZ micropores to reduce the ITZ porosity further. Moreover, the reaction of SF and CH helped to promote the hydration reaction of cement to proceed thoroughly in CPCGA, thus improving CPCGA performance.

1. INTRODUCTION

Coal gangue (CG) is a rock associated with or symbiotic with coal during the formation process of coal resources and discharged as a byproduct by coal mining or separation,[1] which accounts for 10−15% of total raw coal production.[2] At present, the accumulation of CG in China alone exceeds more than 7 billion tons, with 300−350 million tons produced every year,[3] to be the largest single industrial solid waste discharged in China, and a similar situation has occurred in the United States, India, and Australian, and other countries rich in coal reserves.[4,5] CG is an inorganic salt pollutant,[6] especially the rapid environmental change of CG caused by being transported to the surface for disposal from underground accelerates the weathering effect to promote the dissolution of soluble components and aggravate the ecological pollution of CG mounds. The Chinese government has formulated the "Management Measures for Comprehensive Utilization of CG" and encouraged comprehensive utilization of CG resource.[7] Nevertheless, overall utilization rate of CG is less-than 40%,[1] and it is urgent to further improve the utilization of CG in order to eliminate the negative impact on the environment.

CG has a certain amount of application in the construction material,[8] backfill,[9] chemical industry,[10] power generation,[11] chemical fertilizer,[12] but the CG consumption is still much lower than the output in practice resulting in a continuous accumulation of CG,[13] especially in the area of western China.[14] Producing the concrete prepared with CG as an aggregate (CPCGA) is one of the most promising solution for the reason that concrete is currently the largest construction material in the world with approach 17.5 billion tons global annual consumption.[15−17] Generally, the aggregate volume takes up around 70−80% of the concrete volume,[18] which plays an essential role as a "skeleton" in the concrete structures. Natural aggregate used in concrete consists of crushed stone, sand, and gravel from mining natural resources and opening aggregate quarries, is consumed approximately 50 billion tons worldwide per year,[19] which would cause certain disturbances to the environment, and requires an environmentally friendly replacement.[20] Considering all of this, the way to prepare the aggregate with CG could not only reduce the threat to the environment caused by CG but also save natural aggregate resources. Many related research studies have proved that it was feasible and economical to produce concrete using CG as the aggregate. Wang and Zhao[21] showed that the compressive strength of CPCGA after grading adjustment could reach 37 MPa at the age of 28 days. Yao et al.[22] found that the manufacturing cost, energy consumption, and CO_2 emission of asphalt mixture could be decreased by 29.4, 19.8, and 21.9%, respectively, in the case of replacing natural aggregates with 40% reclaimed asphalt pavement coarse aggregate and 25% CG fine aggregate. Nevertheless, the complex mineral composition, weak mechanical properties, and strong water absorption capacity would affect the overall performance of CPCGA, so as

Received: October 30, 2023
Revised: December 13, 2023
Accepted: December 15, 2023
Published: December 27, 2023

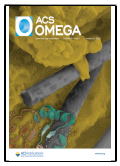

https://doi.org/10.1021/acsomega.3c08560
ACS Omega 2024, 9, 1870−1880

to limit the application of CG.[6,16] Zhou et al.[23] indicated that the CPCGA belonged to the category of low-strength concrete below C30. Gao et al.[20] pointed out that higher steel strength and lower concrete strength should be adopted in preparing concrete-filled steel tubes when employing CG as coarse aggregate.

Concrete is mainly composed of aggregate, matrix, and interfacial transition zone (ITZ) between aggregate and matrix, which is regarded as the weakest part in concrete for the reason that the edge-wall bleeding effect initiated by the surface of aggregate leads to the weak performance of the ITZ compared with the matrix.[24,25] Due to the unique surface properties of CG aggregate, the structure and properties of the ITZ in CPCGA are more unfavorable to improve its mechanical performance than those in natural aggregate concrete, and durability, freezing resistance performance as well.[13,26] Therefore, improving the performance of ITZ is one of the effective ways to improve the performance of concrete,[27] also include CPCGA. Zhu et al.[16] pointed out that CG calcined at 750 °C could significantly enhance the ITZ structure and the strength of concrete, and Yang et al.[28] obtained similar results. Al Khazaleh et al.[29] reported that nanosilica added up to 3% by weight of cement could densify the ITZ to improve the mechanical properties of concrete prepared with 25% CG aggregate. Nevertheless, current investigations have mainly focused on studying the feasibility of CG as concrete aggregate, and less attention has been placed on improving the ITZ in CPCGA, especially lacking the systematic research of weakening the strong water-absorption performance caused by abundant micropores of CG in the concrete hardening process. For this reason, extra admixtures or specific methods were used to avoid the inherent defects of CG is critical to ensure the success of its application.[6]

Silica fume (SF) is also a byproduct from the silicon smelting process in the ferrosilicon and silicon industry with highly pozzolanic activity because of its high amorphous silicon dioxide content and extreme fineness.[30,31] SF could enhance the ITZ of rubberized steel-fiber recycled aggregate concrete,[32] increase the carbonation resistance of self-compacting recycled aggregate concrete,[33] promote the mechanical strength and durability performance,[34] and also lower the adiabatic heat in concrete mass[35] and decrease the chloride binding capacity as well.[36] Studies by Zhang et al.,[37] Mizan et al.,[38] and Ercikdi[39] showed that strong pozzolanic activity of SF could significantly increase the hydration degree of paste. In addition, the active silica in SF could react with $Ca(OH)_2$ (CH) to optimize the ITZ structure, thereby improving the CPCGA performance. Based on the good performance of SF, this paper used SF to improve the performance of ITZ in CPCGA to compensate for the porous structure in the CG aggregate surface and explored the macroscopic properties and microstructure of the ITZ in CPCGA reinforced by SF, which could provide theoretical guidance and technical support for the large-scale utilization of CG in concrete.

2. MATERIALS AND EXPERIMENTAL PROCEDURES

2.1. Materials. The cement used in this study was ordinary Portland cement (OPC) with a strength grade of P.O 42.5 in accordance with the Chinese standard GB 175-2007. The CG was taken from a gangue mound in Guizhou Province, China. X-ray Diffraction (XRD) (Rigaku Smartlab, Rigaku Corporation, Japan) results shown in Figure 1 indicated that CG mainly contained quartz, kaolinite, partheite, jennite, wairakite, gismondine, and other minerals. According to the test results of the scanning electron microscope (SEM) (Zeiss Sigma 300, Zeiss Company, Germany) shown in Figure 2, the CG was a complex mineral aggregate formed by a variety of minerals connected, and noticeable cleavage planes could be seen among all minerals. There existed obvious carbon particles which were not conducive to water transport in the hardening process of paste and durability of concrete.[16] Table 1 lists the chemical composition of the CG explored by X-ray fluorescence (XRF) (Thermo Scientific ARL Perform'X, Thermo Fisher Scientific Co., LTD, America), and the major constituents of the CG were SiO_2 and Al_2O_3, which was similar to that of natural gravel.[20] SF was obtained from a smelter in Henan Province, China. As seen from Table 1, the SiO_2 content in SF reached 91.98%. The XRD peak of SF seen in Figure 1 was almost a straight line with only a slight peak between 15 and 35°, indicating that the SF contained a large amount of amorphous phase, which could be known that SF was mainly composed of active SiO_2 with strong pozzolanic activity from Table 1.[40,41] Figure 3a shows the particle size distributions of the OPC and SF determined by a laser particle size analyzer (LS13320, Beckman Coulter, America), which exhibited that the size range of SF particles was narrower than that of OPC particles. Meanwhile, SF particles were much smaller than the OPC particles from Figure 3b, which was also demonstrated from the SEM images of the OPC and SF shown in Figure 4.

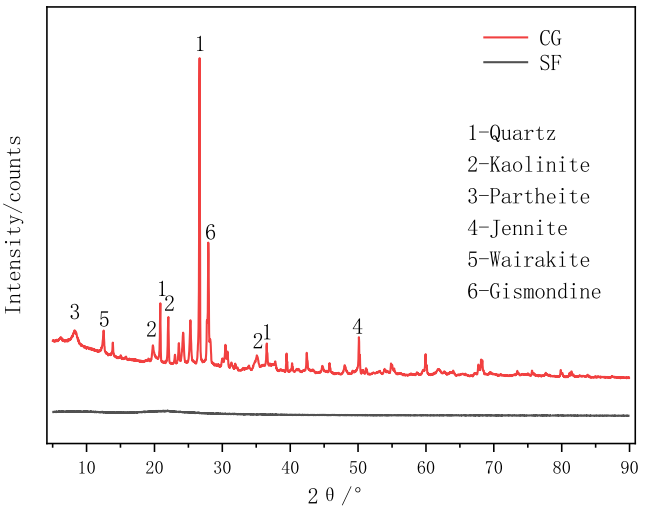

Figure 1. XRD spectra of CG and SF.

2.2. Specimen Preparation. *2.2.1. Preparation of CG Aggregate.* The obvious big coals were picked out by hand from the CG specimen, and tap water was used to clean the CG surface in order to reduce the interference of coal particles attached to the surface of the CG on the test results. The clean CG was dried naturally at room temperature for 3 days, as shown in Figure 5a. A jaw crusher was used for crushing CG to less than 2 mm as CG aggregate in this study, as shown in Figure 5b, and the particle size composition is shown in Table 2.

2.2.2. Preparation of Concrete Specimen. Considering the high water-absorption of the CG aggregate, the water-binder ratio of CPCGA was set to 0.67 and the water reducing agent was added to the mixture in this study, and the detailed mix design proportions of CPCGA added with SF are shown in Table 3. CPCGA specimens were prepared in accordance with

https://doi.org/10.1021/acsomega.3c08560
ACS Omega 2024, 9, 1870−1880

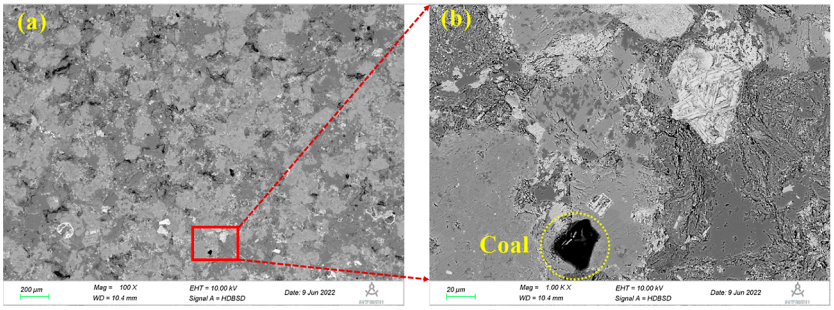

Figure 2. (a) SEM image of CG and (b) enlargement image of area in red box in the (a).

Table 1. Main Chemical Composition of the Raw Materials

	compound/wt %								
materials	SiO_2	CaO	Al_2O_3	TiO_2	Fe_2O_3	MgO	K_2O	Na_2O	P_2O_5
OPC	21.23	61.61	4.32	0.52	3.20	1.88	0.58	0.81	0.25
CG	44.19	2.37	24.17	3.35	4.72	0.949	2.32	2.41	0.395
SF	91.98	0.34	0.32		0.10	0.57	0.12	0.88	

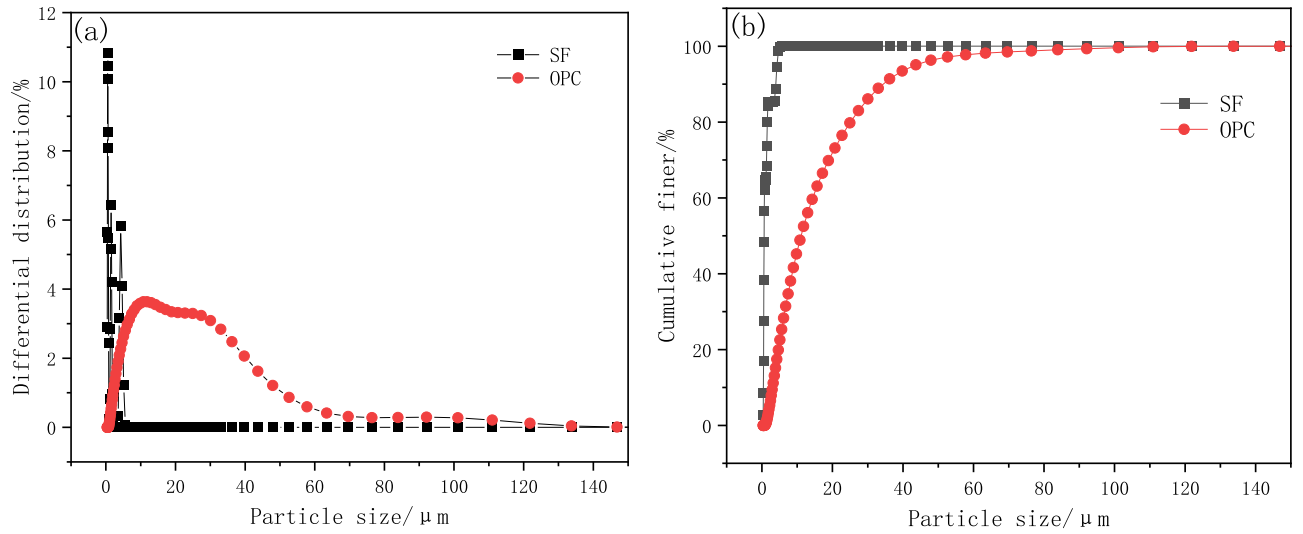

Figure 3. (a) Particle size distributions and (b) grading curves of OPC and SF.

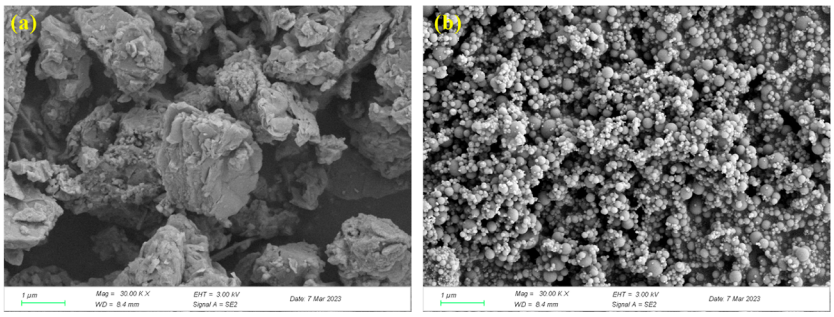

Figure 4. SEM images of (a) OPC and (b) SF.

the Chinese national standard GB/T 17671-2021 (ISO method). The size of the triple mold used in this study was 40 × 40 × 160 mm. The specimen, together with the mold, was put into the curing box for 24 h (humidity ≥90, temperature 20°C ± 1 °C). Then, after demolding, the specimen was placed into the same curing environment and maintained for 7 or 28 days.

2.3. Experimental Methods. *2.3.1. Mechanics Performance Testing.* The flexural strength and the compressive strength of concrete were tested by microcomputer-controlled compression and a flexural tester (YAW-3000B, Zhejiang Yingsong Instrument Equipment Manufacturing Company, Shaoxing city, Zhejiang province, China). For flexural strength testing, the load was evenly applied to the middle of the certain side of the specimen until it broke at a rate of 50 ± 10 N/s.

https://doi.org/10.1021/acsomega.3c08560
ACS Omega 2024, 9, 1870−1880

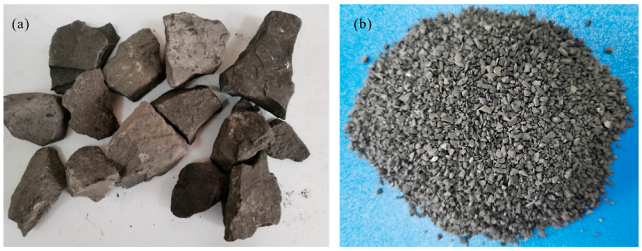

Figure 5. Appearance of (a) cleaning CG and (b) CG aggregate.

Table 2. Particle Size Composition of CG Aggregate

particle size/mm	>2	2−1.6	1.0−0.5	1.6−1.0	<0.5
weight proportion/wt %	0.0	17.8	37.9	44.3	0.0

Then, the three flexural strength R_f (MPa) values obtained according to formula 1 were averaged as the flexural strength of the specimen. For the compressive strength testing, the load was uniformly applied until the specimen was destroyed at a rate of 2400 ± 200 N/s, and the compressive strength R_c (MPa) of the specimen was calculated according to formula 2.[42] Particularly worth mentioning was that the compressive strength of the specimen was the average of those of the six testing blocks.[43]

$$R_f = 1.5 \times F_f \times L/b^3 \quad (1)$$

$$R_c = F_c/b^2 \quad (2)$$

where F_f (N) is the damage load to apply on the middle of the specimen, L (mm) is the distance between the brackets of the tester, b (mm) is the side length of the square cross section of the specimen (40 mm), F_c (N) is the load applied to the specimen when broke.

2.3.2. Microhardness Testing. In this study, the concrete blocks were taken out after curing for 28 days and cut the middle part of the blocks into 15 × 15 mm × 15 mm cube test specimens. The test surface of the specimen was ground step by step by using abrasive papers of 300, 600, 1200, and 2000 mesh. Special attention was given to the quality of the specimen surface polished with alumina oxide polishing powder after grinding so that the aggregate, matrix, and the ITZ could be clearly identified, then soaked in ethanol for 48 h to stop hydration, and placed in an oven (50 °C) to dry until constant weight. The Vickers hardness tester (MVD-JMT, Shanghai Jimin Test Instrument Company, China) was used to test the microhardness of aggregate, matrix, and ITZ, as shown in Figure 6a, under the conditions of reflective observation, load (test force P) = 1000 gf and holding time = 5 s. The test points along the ITZ were designed to reflect the difference in microhardness of aggregate, ITZ, and matrix more accurately, and a schematic presentation of the distribution of hardness data acquisition points is shown in Figure 6b. It was worth mentioning that three specimens for each group were tested, and each specimen was tested ten points, and finally calculated the average value to get more accurate data. The hardness value was calculated by formula 3

$$Hv = 0.102 \times 2F\sin(\alpha/2)/d^2 \quad (3)$$

where F (N) is the load-holding force, α = 136° is the angle between the relative surface of the indenter, and d (mm) is the diagonal length of the indentation.

2.3.3. Porosity Testing of the ITZ. Three cube specimens with side lengths of 10 mm were cut from the location of the geometric center of the concrete test block after curing for 28 days. A representative surface containing aggregate, matrix, and ITZ was selected for grinding and polishing with the same method as that in Section 2.3.2. The specimens were soaked in ethanol for 48 h to stop further hydration and placed in an oven (50 °C) to dry until constant weight. The polished specimen was observed by SEM produced by Zeiss Company in Germany at a magnification of 500 with a low acceleration voltage of 3.00 kV. Ten images containing ITZs were randomly collected for each cube specimen; as a result of that, a total of 30 images were collected for a concrete test block. It was worth mentioning that the aggregate area accounted for less than 1/3 of the total area of the image in each SEM image, while the ITZ and matrix accounted for more than 2/3 to ensure adequate testing area. In this study, the SEM images were used to obtain the ITZ porosity by Image-pro Plus software,[44] and an example of the analysis procedure is shown in Figure 8. A SEM image was binarized, as shown in Figure 7a. The concentric expansion method was employed for strip delineation.[44−46] It was worth mentioning that 10 successive strips with 10 μm width for every image were delineated by adopting the concentric expansion method, as shown in Figure 7b. The black dots of each stripe were counted separately, as shown in Figure 7c for the first stripe, to obtain the corresponding porosity of delineated strips with different distances from the aggregate surface to assess the ITZ porosity.

2.3.4. Porosity Testing of Matrix. The test blocks of cement paste were prepared according to the mix design proportions of w/b, the OPC weight, the SF weight, and the water reducer dosage, as shown in Table 3. The prepared test block was crushed to 5−9 mm as a matrix specimen with a small hammer after curing for 28 days in the curing box (humidity ≥90, temperature 20 ± 1 °C). Furthermore, the prepared specimens were soaked in anhydrous ethanol for 48 h and placed in an oven at 50 °C for approximately 5 h to prevent further hydration. About 20 g representative specimens were selected for each condition. The size and distribution of pores in the matrix were measured by the Mercury Intrusion Porosimetry (MIP) method with the Automatic Mercury Porosimeter (AutoPore IV 9500, Micromeritics Instrument Corporation, America).[47] The relationship between the pressure (p) of

Table 3. Mix Design Proportions of CPCGA Added with SF

specimens	water-binder ratio (w/b)	OPC weight/g	SF weight/g	water reducer/mL	aggregate weight/g	aggregate density/($\times 10^3$ kg·m^3)	aggregate size/mm
100P-0S		450.00	0.00				
97.5P-2.5S		438.75	11.25				
95P-5S	0.67	427.50	22.50	7			
92.5P-7.5S		416.25	33.75				
90P-10S		405.00	45.00				

https://doi.org/10.1021/acsomega.3c08560
ACS Omega 2024, 9, 1870−1880

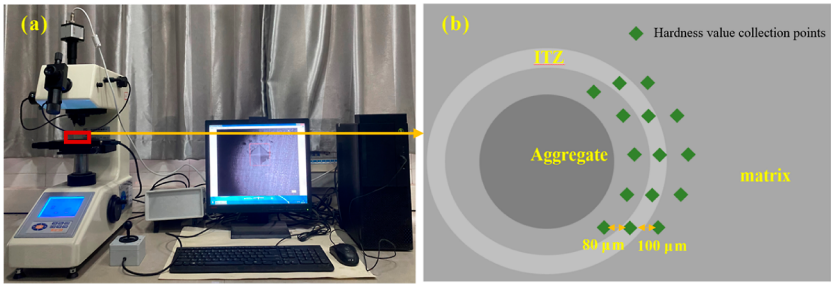

Figure 6. (a) Picture microhardness tester and (b) schematic presentation of the distribution of hardness data acquisition points.

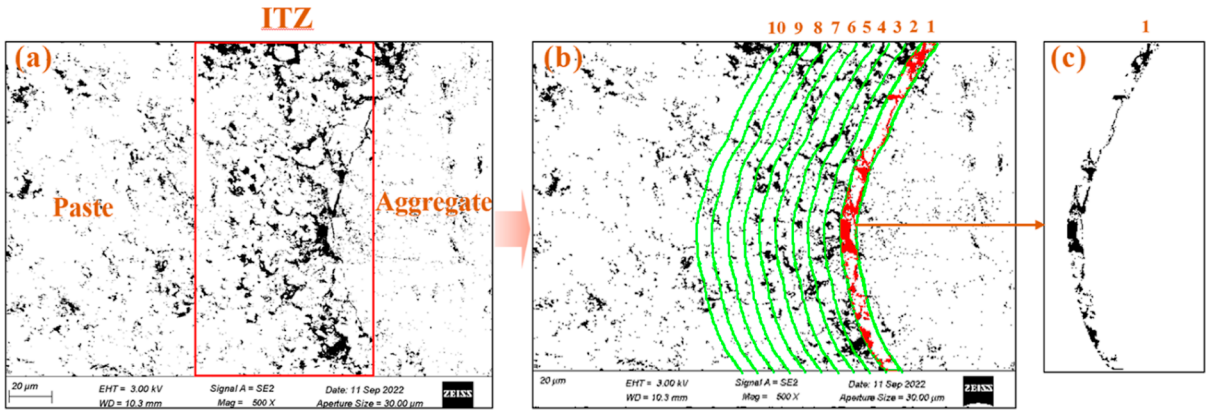

Figure 7. Example of the SEM image analysis procedure: (a) the binary image of SEM image; (b) images of different gray levels of the zone in the red box in the image (b,c) image with successive strips.

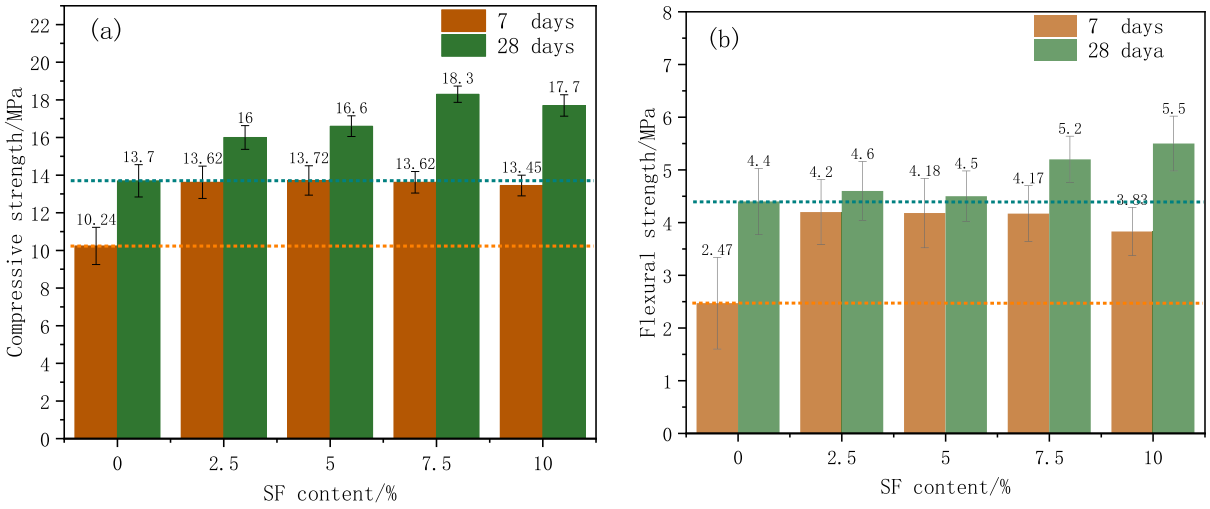

Figure 8. (a) Compressive strength and (b) flexural strength of CPCGA added to different content SF.

mercury injected into the pore, and the pore radius R (nm) was as follows

$$R = (2 \times \sigma \times \cos \beta)/p \quad (4)$$

where σ is the surface tension of mercury, β is the wetting angle between the specimen and mercury, and p is the injection pressure. It is worth noting that the mercury was pressed into the pore of the specimen. The radius of the pore could be obtained according to P and the size, and total area of the pore could be confirmed.[48]

2.3.5. Microscopic Morphology of ITZ. The specimen preparation process was the same as that described in Section 2.3.3. The surfaces containing the aggregate, matrix, and ITZ of the test specimens were gilded before testing to prevent the charge from affecting the test results. The microstructure and morphology of ITZ in concrete were observed by adopting SEM produced by Zeiss Company in Germany at the 2000× magnification and 10 000× magnification, respectively, with a low acceleration voltage of 3.00 kV.

3. RESULTS AND DISCUSSION

3.1. Mechanical Properties. The compressive strength and flexural strength were the most direct and necessary indexes to measure concrete performance,[3] which were employed to characterize the influence of SF on the mechanical properties of concrete in this study, and the test

https://doi.org/10.1021/acsomega.3c08560
ACS Omega 2024, 9, 1870−1880

results are shown in Figure 8. Both the flexural strength and the compressive strength of the CPCGA in the presence of SF increased obviously no matter at the age of 7 or 28 days, indicating that the suitable amount of SF could promote the mechanical properties of CPCGA. With increasing SF content, the compressive strength of CPCGA showed a trend of increasing gradually at first and then decreasing slowly, especially for the 7 days compressive strength. Compared with the 28 days compressive strength of the 100P-0S specimen, the compressive strength of 97.5P-2.5S, 95P-5S, 92.5P-7.5S, and 90P-10S increased by 16.79, 21.17, 33.58, and 29.20%, respectively. It could be seen from Figure 8a that the optimal SF mixing amount was 5% when the 7 days compressive strength was taken as the analytical standard. In comparison, the optimal SF mixing amount moved to 7.5% when 28 days compressive strength was taken, which could be attributed to the low reaction activity of SF at early ages.[37] Nevertheless, the compressive strength of CPCGA gradually decreased with the increasing SF content because excess SF reduced the cement content and thus reduced the content of the hydration products of cement, especially calcium silicate hydrate (C−S−H) and CH, and then insufficient CH further reacted with active SiO_2 in SF. In other words, the critical SF dose added to CPCGA could significantly improve the interfacial bond strength.[49]

As seen from Figure 8b, the changing rule of the flexural strength at the age of 7 days was similar to that of the compressive strength with increasing SF content, while it showed a gradually increasing trend at the age of 28 days. The flexural strength of the 97.5P-2.5S, 95P-5S, 92.5P-7.5S, and 90P-10S increased by 4.55, 2.27, 18.18, 25.00% at the age of 28 days compared with the 28 days flexural strength of 100P-0S specimen, which indicated that SF had a significant promoting effect on the mechanical properties of the ITZ of CPCGA for the reason that the flexural strength of specimen was considered to be a representation of the bonding strength between matrix and aggregate.[37] This phenomenon meant that SF had played a significant role in improving the structure characteristics of the ITZ as a result of the bond strength of ITZ being related to the ITZ characteristics based on the previous researches.[44,50]

3.2. Microhardness of the ITZ. Microhardness is a comprehensive parameter used to reflect the information of material microstructure to well character the microstructure evolution and mechanical property of material, including cementitious materials.[51,52] In this study, the microhardness was employed to characterize the influence of different dosages of SF on the properties of the ITZ in CPCGA. The change in matrix hardness was also tested, as shown in Figure 9. In particular, the control group of CPCGA without SF was designed in order to reflect better the difference of CPCGA affected by SF. As seen in Figure 9, the hardness of CG was low, even lower than that of ITZ, and it was the inherent defect as concrete aggregate, which was similar to the conclusions of previous researches.[53,54] The primary reason might lie in a small number of coal particles and many aluminosilicate minerals with less hardness, such as Kaolinite, Partheite, Jennite, Wairakite, and Gismondin known from Figures 1 and 2. The low-strength aggregate is very unfavorable to the concrete performance.[55] Therefore, it was necessary to consider the application fields of CPCGA. The microhardness generally increased first and then decreased with increasing SF dosage, which implied that there was also an optimal SF

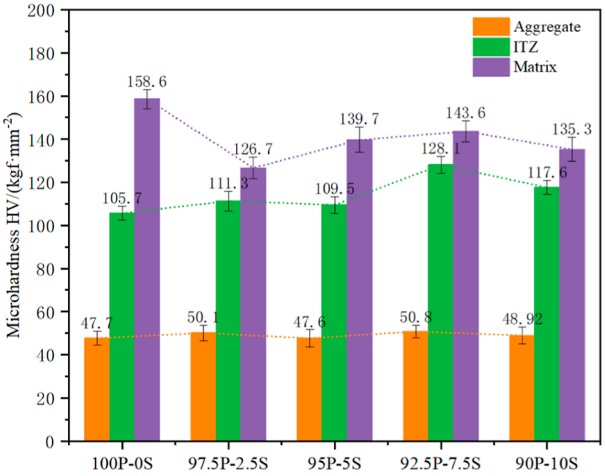

Figure 9. Microhardness value of aggregate, matrix, and ITZ in CPCGA added different content SF.

content to improve the microhardness of the ITZ in the CPCGA. Moreover, the hardness increased by 21.19% in the presence of 7.5% SF, which indicated that SF acting as a pozzolanic microfiller in concrete improved the hardness of the ITZ in the CPCGA. The reason for this observation might lie in reducing the size of the capillary pores in concrete,[56] adjusting the CH crystal orientation index, and improving the pore microstructure,[57,58] thereby making the ITZ denser than that of the control group. It could also be noted that the microhardness of the matrix decreased slightly after the addition of SF with no apparent regularity. This was mainly because the quantity of bleed water and water absorption values was significantly reduced in the presence of SF.[59] In addition, adding SF might decrease the thickness of the ITZ to increase the overall mechanical properties of CPCGA.[49] These results were in agreement with the testing results of the mechanical properties above.

3.3. Porosity of the ITZ. Compacting the ITZ structure to reduce the size and number of micropores is an effective way to improve the mechanical properties of concrete. The concrete specimens of 100P-0S, 92.5P-7.5S, and 90P-10S were selected to test the porosity and the maximum micropore area of profile starting from the CG aggregate surface to judge the influence of SF on the ITZ compactness in CPCGA. In this study, we defined D_{fa} as the distance from the aggregate surface to express the relevance well. Curves were made and fitted according to the experimental data to show the relationship between the porosity and D_{fa}, as shown in Figures 10 and 11, respectively.

As seen from Figure 10, the porosity of 100P-0S decreased rapidly with the gradual increase of the D_{fa}, and the porosity began to decline slowly and finally approached a fixed value when D_{fa} exceeded 70 μm. The porosity of ITZ in 92.5P-7.5S decreased more slowly with increasing D_{fa} compared with 100P-0S, and the reduction rate of porosity began to decline when D_{fa} was more than 50 μm. Moreover, the porosity of ITZ in 92.5P-7.5S decreased by 44.22, 46.16, and 24.46% at the D_{fa} of 10, 50, and 100 μm compared with 100P-0S, respectively. The results confirmed that the addition of SF could effectively reduce the size and number of pores in the ITZ. It is well-known that the cement hydration process involves many complex chemical reactions. CH is one of the main hydration products of tricalcium silicate (C_3S) and dicalcium silicate

https://doi.org/10.1021/acsomega.3c08560
ACS Omega 2024, 9, 1870−1880

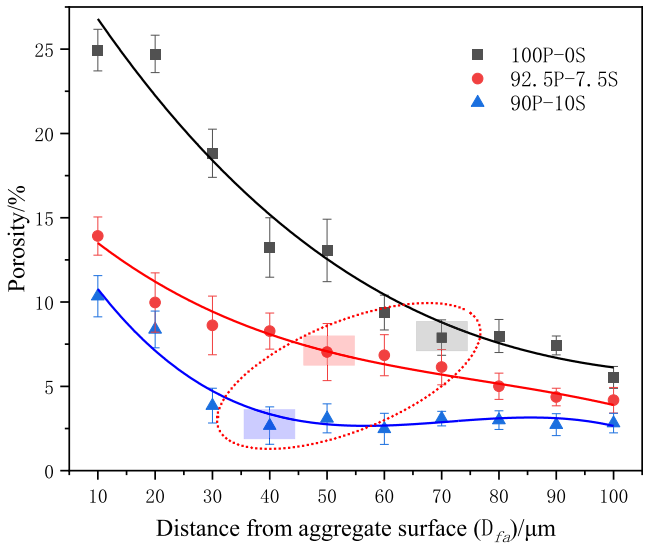

Figure 10. Porosity of the profile starting from the CG aggregate surface in 100P-0S, 92.5P-7.5S, and 90P-10S.

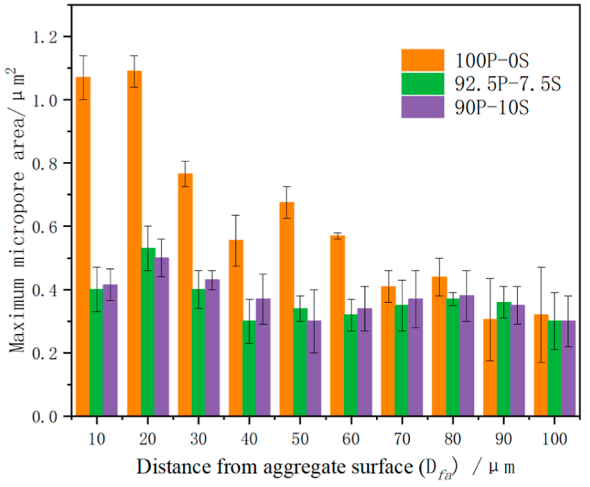

Figure 11. Maximum micropore area of the profile starting from the CG aggregate surface in 100P-0S, 92.5P-7.5S, and 90P-10S.

(C_2S), which are the main components in cement, as shown in formulas 5 and 6, and CH exists in the ITZ of concrete in large quantities.[47] A large amount of active SiO_2 in SF reacted with coarse CH crystals in the ITZ to reduce the large apertures caused by coarse CH and oriented CH crystals, as shown in formula 7.[60] In addition, the generated C−S−H gel could fill the micropores near aggregates to further contribute to the reduction in pore size and number in the ITZ.[61] It should also be noted that amorphous SiO_2 reacted with CH to produce C−S−H gel to promote full completion of the cement hydration reaction.[62] The change in porosity in 90P-10S was similar to that in 92.5P-7.5S, except that the porosity in 90P-10S almost no longer decreased when D_{fa} reached 40 μm. Additionally, adding SF compressed the thickness of the ITZ from 70 to <40 μm, which helped to improve the fracture strength of the CPCGA.

$$2C_3S + 6H_2O \rightarrow 3C-S-H + 3CH \quad (5)$$

$$2C_2S + 4H_2O \rightarrow 3C-S-H + CH \quad (6)$$

$$\text{active } SiO_2 + CH \rightarrow C-S-H + H_2O \quad (7)$$

Figure 11 demonstrates that the addition of SF effectively reduced the size of the maximum aperture. It is worth noting that the maximum pore size did not continue to decrease in the presence of an SF amount exceeding 7.5%. The main reason might be that the active SiO_2 in SF could not get enough CH to react when excessive SF was added, resulting in the formation of large pores around the big SF particles to lead to the large pore. Therefore, a 7.5% SF dosage was suitable to optimize the microstructure of CPCGA.

Based on the experimental results, it could be preliminarily concluded that SF particles near the aggregate surface and CG aggregate micropores competitively adsorbed water near the aggregate, resulting in less mixed water inhaled into the pores of CG than that without SF, which weakened the adverse effect of the porous surface of CG on CPCGA; furthermore, active SiO_2 could react with CH in the ITZ as described above in the hydration process. The two reasons above mainly contributed to the dense ITZ and narrow ITZ width in CPCGA with SF, and schematic illustrations of the influence of SF on the ITZ in CPCGA are shown in Figure 12.

3.4. Micropore Structure of the Matrix. As mentioned above, the size, number, and distribution of micropores in concrete have significant influence on CPCGA performance. As an essential component of concrete, the porosity and pore size distribution in the matrix also needed to be concerned for the reason that the volume of matrix was much larger than that of ITZ. It was known that there were a large number of different pore diameter micropores with nonuniform distribution inside the concrete, and different pore size micropores had different effects on concrete performances. For example, micropores with less than 20 nm diameter are not harmful to concrete performances, micropores with 20−100 nm diameter have a little effect on concrete performances and micropores with more than 100 nm diameter are considered harmful to concrete performances.[63] The MIP test was used in order to explain the effect of the SF on the pore size of matrix in CPCGA. Approximately rough 3 g of specimens from the 20 g representative specimens were tested with the parameters set at 485 dyn/cm for Hg surface tension and 130 for contact Angle,[64] and the test results are shown in Table 4. The total

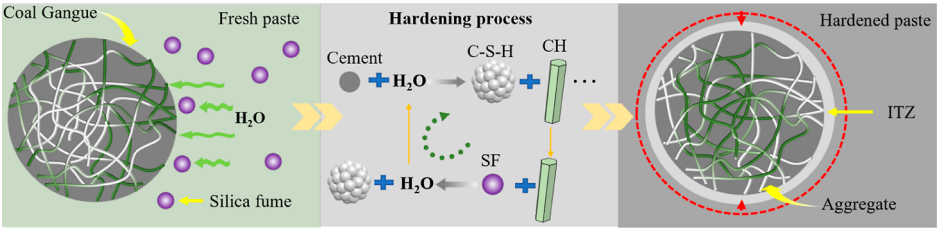

Figure 12. Schematic illustrations of the influence of SF on ITZ in CPCGA.

https://doi.org/10.1021/acsomega.3c08560
ACS Omega 2024, 9, 1870−1880

Table 4. Micropore of the Matrix in CPCGA

group	total pore area/m^2/g	average pore diameter (4 V/A)/nm	median pore diameter (volume)/nm	porosity/%
100P-0S	8.51	15.07	22.78	6.03
92.5P-7.5S	5.22	8.57	10.53	4.88
90P-10S	5.85	10.63	16.43	4.02

pore area, average pore diameter, median pore diameter, and porosity of the matrix in 100P-0S were 8.51 m^2/g, 15.07/nm, 22.78 nm, and 6.03%, respectively, which were all greater than those of 92.5P-7.5S or 90P-10S. In particular, the total pore area, average pore diameter, median pore diameter, and porosity of the matrix in 92.5P-7.5S were reduced by 38.66, 43.53, 53.75, and 19.07%, respectively, compared with those in 100P-0S. These results indicated that SF also played an essential role in optimizing the pore structure of the matrix. As with the effect of SF on the ITZ, the active SiO_2 in SF reacted with CH described in formula 7, and the matrix was filled with inactive fine particles simultaneously. It was remarkable that the average pore diameter and median pore diameter in 90P-10S were obviously larger than the corresponding values of 92.5P-7.5S, indicating that 10% SF tended to be excessive.

3.5. Morphology and Structure of the ITZ. The ITZs in CPCGA of 100P-0S, 92.5P-7.5S, and 90P-10S were selected to observe the 7.5% SF content according to the research results above. The representative SEM images of ITZ were shown in Figure 13. There were many micropores and cracks in the ITZs of the 100P-0S specimen, and there were also a large number of spherical or spheroidal particles with loose shape. It was worth noting that there were wide interspaces between CH crystals when observed at 10 000× magnification, which was not conducive to the durability, corrosion resistance and mechanical properties of concrete,[44] was prone to microcrack underloading, and led to a transformation of the linear response to the nonlinear response as well.[42] The particle size in the ITZ of the 92.5P-7.5S specimen was significantly reduced at 10 000× magnification, and there existed small CH particles instead of loose CH crystals. Moreover, the size of

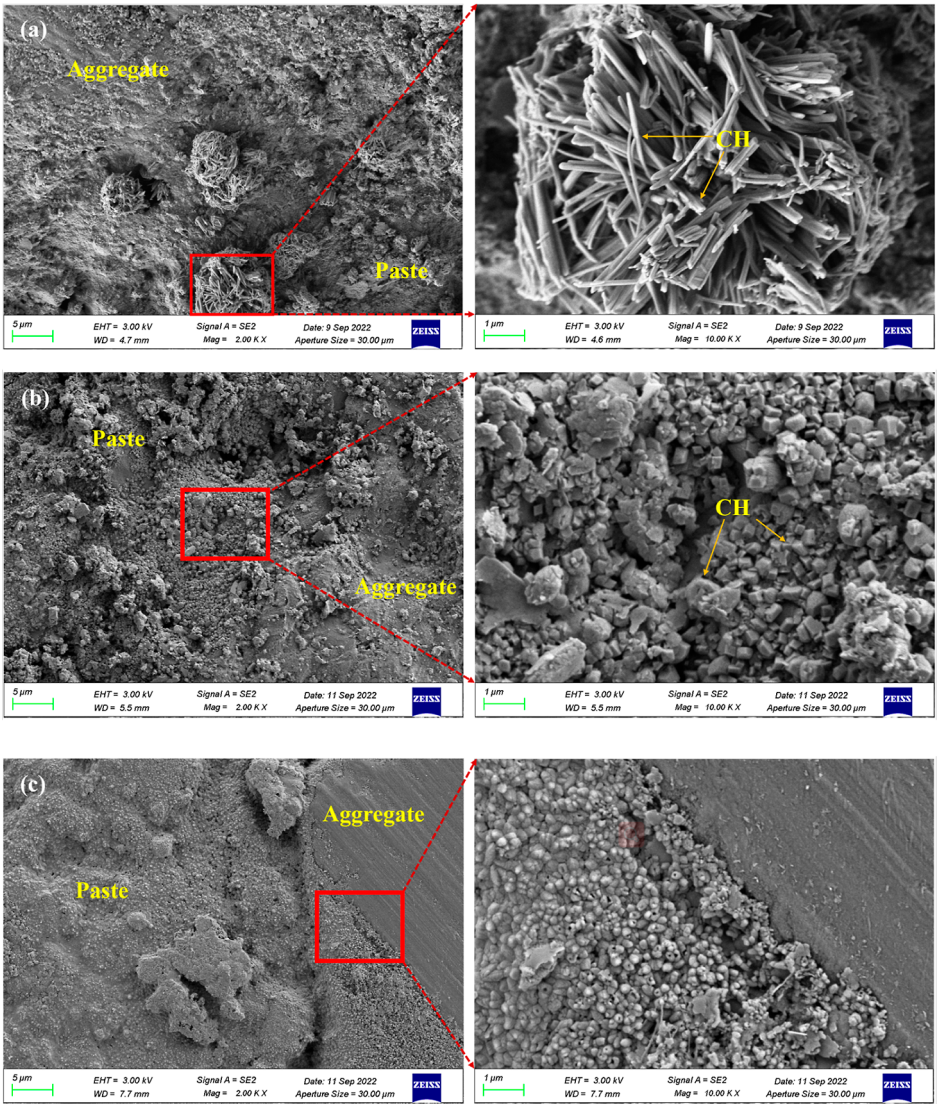

Figure 13. Representative images of ITZ in CPCGA of (a) 100P-0S, (b) 92.5P-7.5S, and (c) 90P-10S (the images on the left were observed at 2000× magnification, and images on the right were enlargements of areas in red boxes in left images, respectively).

https://doi.org/10.1021/acsomega.3c08560
ACS Omega 2024, 9, 1870−1880

micropore around CH was significantly reduced, and part of the large pores were filled with small particulate matter, which contributed to the reaction between SF and CH in the ITZ that occurred as shown in Formula 7 to generate the C−S−H gel to fill the pores. In the meantime, a large amount of CH was consumed to reduce the large pore size caused by the coarse CH in the ITZ.[65] The above two reasons together led to the high density of the ITZ, and these results were consistent with the results of the ITZ analysis. Figure 13c shows that the ITZ morphology of many relatively small particles was obviously different from those of Figure 13a,b as the SF content increased to 10%. Furthermore, this observation was more obvious at 10 000× magnification. It was possible that the unreacted particles in SF also filled pores in the ITZ in addition to active particles reacting with CH because SF has also been determined to be a well-filling material due to its small size and spherical particle shape.[66,67]

4. CONCLUSIONS

This article adopted SF to strengthen the performance of the ITZ in CPCGA and focused on the macroscopic properties and microstructure of the ITZ in CPCGA with SF. The following conclusions were drawn:

1 The compressive strength of CPCGA prepared with cement replaced by a 7.5% mass ratio of SF at the age of 28 days increased by more than 30%, and the flexural strength increased by over 20%.
2 The ITZ hardness could be improved in the presence of a 7.5% mass ratio of SF in the cementing material in CPCGA.
3 SEM imaging of the ITZ analyzed by Image-pro Plus software was a suitable method to obtain information regarding micropore size distribution.
4 SF could effectively reduce the porosity and micropore size in the ITZ of CPCGA, and the porosity of the ITZ in CPCGA with 7.50% SF decreased by 44.22, 46.16, and 24.46% at distances from the aggregate surface of 10, 50, and 100 μm, respectively, compared to CPCGA without SF.
5 The reaction involved in active substances in SF during the hardening process contributed to a dense ITZ and narrow ITZ width of CPCGA by adding SF.
6 The CH generated in the cement hydration reaction reacted with a large amount of active SiO_2 from SF to make it difficult to form coarse CH in the ITZ of CPCGA. The generated C−S−H gel filled the ITZ micropores to further reduce the ITZ porosity.
7 The reaction of SF and CH helped to promote the further hydration reaction of cement forward to react thoroughly in CPCGA, thus improving CPCGA performance.

AUTHOR INFORMATION

Corresponding Author

Xianhai Li − *Mining College, Guizhou University, Guiyang 550025, China*; orcid.org/0000-0002-5348-7524; Email: xhli1@gzu.edu.cn

Authors

Xianchen Wang − *Moutai Institute, Renhuai 564507, China*
Yanxia Zhong − *Moutai Institute, Renhuai 564507, China*
Hong Li − *Moutai Institute, Renhuai 564507, China*
Jie Wang − *School of Minerals Processing & Bioengineering, Central South University, Changsha 410083, China*

Complete contact information is available at: https://pubs.acs.org/10.1021/acsomega.3c08560

Author Contributions

The manuscript was written through the contributions of all authors. All authors have approved the final version of the manuscript.

Notes

The authors declare no competing financial interest.

ACKNOWLEDGMENTS

The authors would like to acknowledge the Project of Moutai Institute High-level Talent Scientific Research (mygccrc[2022]062 and mygccrc[2022]028), the Cultivation Project of Guizhou University, China (no. [2020] 29), the Project of Department of Education of Guizhou Province (Qian Jiao Ji [2022]411), and the Project supported by the Research Foundation of Education of Zunyi [Zun Shi Ke He HZ Zi (2021)323 and (2022)176] for their financial support to the work presented in this paper.

REFERENCES

(1) Jin, Y.; Liu, Z.; Han, L.; Zhang, Y.; Li, L.; Zhu, S.; Li, Z. P. J.; Wang, D. Synthesis of coal-analcime composite from coal gangue and its adsorption performance on heavy metal ions. *J. Hazard. Mater.* **2022**, *423*, 127027.
(2) Qin, L.; Gao, X. Properties of coal gangue-Portland cement mixture with carbonation. *Fuel* **2019**, *245*, 1−12.
(3) Ma, H.; Zhu, H.; Wu, C.; Chen, H.; Sun, J.; Liu, J. Study on compressive strength and durability of alkali-activated coal gangue-slag concrete and its mechanism. *Powder Technol.* **2020**, *368*, 112−124.
(4) Cheng, Y.; Hongqiang, M.; Hongyu, C.; Jiaxin, W.; Jing, S.; Zonghui, L.; Mingkai, Y. Preparation and characterization of coal gangue geopolymers. *Constr. Build. Mater.* **2018**, *187*, 318−326.
(5) Zhang, X.; Li, C.; Zheng, S.; Di, Y.; Sun, Z. A review of the synthesis and application of zeolites from coal-based solid wastes. *Int. J. Miner., Metall. Mater.* **2022**, *29* (1), 1−21.
(6) Gao, S.; Zhang, S.; Guo, L. Application of Coal Gangue as a Coarse Aggregate in Green Concrete Production: A Review. *Materials* **2021**, *14* (22), 6803.
(7) Zhang, Y.; Ling, T. Reactivity activation of waste coal gangue and its impact on the properties of cement-based materials - A review. *Constr. Build. Mater.* **2020**, *234*, 117424.
(8) Zhang, N.; Li, H.; Liu, X. Hydration kinetics of cementitious materials composed of red mud and coal gangue. *Int. J. Miner., Metall. Mater.* **2016**, *23* (10), 1215−1224.
(9) Li, M.; Zhang, J.; Li, A.; Zhou, N. Reutilisation of coal gangue and fly ash as underground backfill materials for surface subsidence control. *J. Cleaner Prod.* **2020**, *254*, 120113.
(10) Li, B.; Gong, G.; Xie, B.; Yang, W.; Yang, M.; Lai, S. Fracture behaviour of polypropylene sheets filled with epoxidized natural rubber (ENR)-treated coal gangue powder. *J. Mater. Sci.* **2007**, *42* (11), 3856−3864.
(11) Zhang, Y.; Zhang, Z.; Zhu, M.; Cheng, F.; Zhang, D. Decomposition of key minerals in coal gangues during combustion in O2/N2 and O2/CO2 atmospheres. *Appl. Therm. Eng.* **2019**, *148*, 977−983.
(12) Zhou, C.; Liu, G.; Cheng, S.; Fang, T.; Lam, P. K. S. Thermochemical and trace element behavior of coal gangue, agricultural biomass and their blends during co-combustion. *Bioresour. Technol.* **2014**, *166*, 243−251.

(13) Hao, Y.; Guo, X.; Yao, X.; Han, R.; Li, L.; Zhang, M. Using Chinese Coal Gangue as an Ecological Aggregate and Its Modification: A Review. *Materials* **2022**, *15* (13), 4495.
(14) Zhang, Y.; Yang, Y.; Zeng, Q. Research on Coal Gangue Recognition Based on Multi-source Time-Frequency Domain Feature Fusion. *ACS Omega* **2023**, *8* (28), 25221−25235.
(15) Wu, B.; Yu, Y.; Chen, Z.; Zhao, X. Shape effect on compressive mechanical properties of compound concrete containing demolished concrete lumps. *Constr. Build. Mater.* **2018**, *187*, 50−64.
(16) Zhu, Y.; Zhu, Y.; Wang, A.; Sun, D.; Liu, K.; Liu, P.; Chu, Y. Valorization of calcined coal gangue as coarse aggregate in concrete. *Cem. Concr. Compos.* **2021**, *121*, 104057.
(17) Zhang, T.; Zhang, Y.; Wang, Q.; Aganyira, A. K.; Fang, Y. Experimental study and machine learning prediction on compressive strength of spontaneous-combustion coal gangue aggregate concrete. *J. Build. Eng.* **2023**, *71*, 106518.
(18) Verian, K. P.; Ashraf, W.; Cao, Y. Properties of recycled concrete aggregate and their influence in new concrete production. *Resour., Conserv. Recycl.* **2018**, *133*, 30−49.
(19) Liu, Y.; Ling, T.; Mo, K. Progress in developing self-consolidating concrete (SCC) constituting recycled concrete aggregates: A review. *Int. J. Miner., Metall. Mater.* **2021**, *28* (4), 522−537.
(20) Gao, S.; Zhao, G.; Guo, L.; Zhou, L.; Yuan, K. Utilization of coal gangue as coarse aggregates in structural concrete. *Constr. Build. Mater.* **2021**, *268*, 121212.
(21) Wang, Z.; Zhao, N. Influence of coal gangue aggregate grading on strength properties of concrete. *Wuhan Univ. J. Nat. Sci.* **2015**, *20* (1), 66−72.
(22) Yao, Y.; Gao, J.; Yang, J.; Huang, B.; Song, L. Sustainable Asphalt Concrete Containing RAP and Coal Gangue Aggregate: Performance, Costs, and Environmental Impact. *J. Renewable Mater.* **2022**, *10* (8), 2263−2285.
(23) Zhou, M.; Dou, Y.; Zhang, Y.; Zhang, Y.; Zhang, B. Effects of the variety and content of coal gangue coarse aggregate on the mechanical properties of concrete. *Constr. Build. Mater.* **2019**, *220*, 386−395.
(24) Husem, M. The effects of bond strengths between lightweight and ordinary aggregate-mortar, aggregate-cement paste on the mechanical properties of concrete. *Mater. Sci. Eng., A* **2003**, *363* (1−2), 152−158.
(25) Rossignolo, J. A.; Rodrigues, M. S.; Frias, M.; Santos, S. F.; Junior, H. S. Improved interfacial transition zone between aggregate-cementitious matrix by addition sugarcane industrial ash. *Cem. Concr. Compos.* **2017**, *80*, 157−167.
(26) LI, Y.-J.; Geng, X.; Zhang, X.; Yan, X. Experimental study on the durability of the concrete with coal gangue aggregate. *J. China Coal Soc.* **2013**, *38* (07), 1215−1219.
(27) Abdelsattar, D. E.; El-Demerdash, S. H.; Zaki, E. G.; Dhmees, A. S.; Azab, M. A.; Elsaeed, S. M.; Kandil, U. F.; Naguib, H. M. Effect of Polymer Waste Mix Filler on Polymer Concrete Composites. *ACS Omega* **2023**, *8* (42), 39730−39738.
(28) Yang, Q.; Lü, M.; Luo, Y. Effects of surface-activated coal gangue aggregates on properties of cement-based materials. *J. Wuhan Univ. Technol.* **2013**, *28* (6), 1118−1121.
(29) Al Khazaleh, M.; Kumar, P. K.; Mohamed, M. J. S.; Kandasamy, A. Influence of coarse coal gangue aggregates on properties of structural concrete with nano silica. *Mater. Today: Proc.* **2022**, *72*, 2089.
(30) Siddique, R. Utilization of silica fume in concrete: Review of hardened properties. *Resour., Conserv. Recycl.* **2011**, *55* (11), 923−932.
(31) Nazeer, M.; Kapoor, K.; Singh, S. P. Strength, durability and microstructural investigations on pervious concrete made with fly ash and silica fume as supplementary cementitious materials. *J. Build. Eng.* **2023**, *69*, 106275.
(32) Xie, J.; Fang, C.; Lu, Z.; Li, Z.; Li, L. Effects of the addition of silica fume and rubber particles on the compressive behaviour of recycled aggregate concrete with steel fibres. *J. Cleaner Prod.* **2018**, *197*, 656−667.
(33) Singh, N.; Singh, S. P. Carbonation resistance of self-compacting recycled aggregate concretes with silica fume. *J. Sustainable Cem.-Based Mater.* **2018**, *7* (4), 214−238.
(34) Nili, M.; Ehsani, A. Investigating the effect of the cement paste and transition zone on strength development of concrete containing nanosilica and silica fume. *Mater. Des.* **2015**, *75*, 174−183.
(35) Awal, A. A.; Shehu, I. A. Evaluation of heat of hydration of concrete containing high volume palm oil fuel ash. *Fuel* **2013**, *105*, 728−731.
(36) Guo, Y.; Zhang, T.; Tian, W.; Wei, J.; Yu, Q. Physically and chemically bound chlorides in hydrated cement pastes: a comparison study of the effects of silica fume and metakaolin. *J. Mater. Sci.* **2019**, *54* (3), 2152−2169.
(37) Zhang, Z.; Zhang, B.; Yan, P. Comparative study of effect of raw and densified silica fume in the paste, mortar and concrete. *Constr. Build. Mater.* **2016**, *105*, 82−93.
(38) Mizan, M. H.; Ueda, T.; Matsumoto, K. Enhancement of the concrete-PCM interfacial bonding strength using silica fume. *Constr. Build. Mater.* **2020**, *259*, 119774.
(39) Ercikdi, B.; Cihangir, F.; Kesimal, A.; Deveci, H.; Alp, İ. Utilization of industrial waste products as pozzolanic material in cemented paste backfill of high sulphide mill tailings. *J. Hazard. Mater.* **2009**, *168* (2−3), 848−856.
(40) Wongkeo, W.; Chaipanich, A. Compressive strength, microstructure and thermal analysis of autoclaved and air cured structural lightweight concrete made with coal bottom ash and silica fume. *Mater. Sci. Eng., A* **2010**, *527* (16−17), 3676−3684.
(41) Nmiri, A.; Duc, M.; Hamdi, N.; Yazoghli-Marzouk, O.; Srasra, E. Replacement of alkali silicate solution with silica fume in metakaolin-based geopolymers. *Int. J. Miner., Metall. Mater.* **2019**, *26* (5), 555−564.
(42) Li, X.; Zhang, Q.; Mao, S. Investigation of the bond strength and microstructure of the interfacial transition zone between cement paste and aggregate modified by Bayer red mud. *J. Hazard. Mater.* **2021**, *403*, 123482.
(43) Gu, X.; Sun, W.; Ai, Y. Application of Copper Slag in Ultra-high Performance Concrete. *JOM* **2023**, *75* (4), 1059−1067.
(44) Zhang, L.; Zhang, Y.; Liu, C.; Liu, L.; Tang, K. Study on microstructure and bond strength of interfacial transition zone between cement paste and high-performance lightweight aggregates prepared from ferrochromium slag. *Constr. Build. Mater.* **2017**, *142*, 31−41.
(45) Chen, H.; Zhu, Z.; Liu, L.; Sun, W.; Miao, C. Aggregate shape effect on the overestimation of ITZ thickness: Quantitative analysis of Platonic particles. *Powder Technol.* **2016**, *289*, 1−17.
(46) Zhu, Z.; Chen, H. Overestimation of ITZ thickness around regular polygon and ellipse aggregate. *Comput. Struct.* **2017**, *182*, 205−218.
(47) Su, Z.; Li, X.; Zhang, Q. Influence of thermally activated coal gangue powder on the structure of the interfacial transition zone in concrete. *J. Cleaner Prod.* **2022**, *363*, 132408.
(48) Cheng, A.; Hsu, H.; Chao, S. Properties of concrete incorporating bed ash from circulating fluidized bed combustion and ground granulates blast-furnace slag. *J. Wuhan Univ. Technol.* **2011**, *26* (2), 347−353.
(49) Xuan, D. X.; Shui, Z. H.; Wu, S. P. Influence of silica fume on the interfacial bond between aggregate and matrix in near-surface layer of concrete. *Constr. Build. Mater.* **2009**, *23* (7), 2631−2635.
(50) Kuroda, M.; Watanabe, T.; Terashi, N.; Gumma Univ, K. J. Increase of bond strength at interfacial transition zone by the use of fly ash. *Cem. Concr. Res.* **2000**, *30* (2), 253−258.
(51) Hu, C.; Li, Z. A review on the mechanical properties of cement-based materials measured by nanoindentation. *Constr. Build. Mater.* **2015**, *90*, 80−90.
(52) Venkovic, N.; Sorelli, L.; Martirena, F. Nanoindentation study of calcium silicate hydrates in concrete produced with effective microorganisms-based bioplasticizer. *Cem. Concr. Compos.* **2014**, *49*, 127−139.

https://doi.org/10.1021/acsomega.3c08560
ACS Omega 2024, 9, 1870−1880

(53) Luo, D.; Wang, Y.; Zhang, S.; Niu, D.; Song, Z. Frost Resistance of Coal Gangue Aggregate Concrete Modified by Steel Fiber and Slag Powder. *Appl. Sci.* **2020**, *10* (9), 3229.
(54) Wang, Q.; Li, Z.; Zhang, Y.; Zhang, H.; Zhou, M.; Fang, Y. Influence of coarse coal gangue aggregates on elastic modulus and drying shrinkage behaviour of concrete. *J. Build. Eng.* **2020**, *32*, 101748.
(55) Lu, J.; Shen, P.; Ali, H. A.; Poon, C. S. Mix design and performance of lightweight ultra high-performance concrete. *Mater. Des.* **2022**, *216*, 110553.
(56) Rao, G. A.; Prasad, B. K. R. Influence of the roughness of aggregate surface on the interface bond strength. *Cem. Concr. Res.* **2002**, *32* (2), 253−257.
(57) Qudoos, A.; Atta-ur-Rehman Kim, H. G.; Kim, H. G.; Ryou, J. S. Influence of the surface roughness of crushed natural aggregates on the microhardness of the interfacial transition zone of concrete with mineral admixtures and polymer latex. *Constr. Build. Mater.* **2018**, *168*, 946−957.
(58) Shui, Z. H.; Zeng, J. J.; Liao, Y.; Leng, Z. Influence of Metakaolin on Strength and Microstructure of High-Strength Concrete. *Key Eng. Mater.* **2012**, *509*, 33−39.
(59) Nolan, E.; Basheer, P. A. M.; Long, A. E. Effects of three durability enhancing products on some physical properties of near surface concrete. *Constr. Build. Mater.* **1995**, *9* (5), 267−272.
(60) Chen, J.; Zhao, B.; Wang, X.; Zhang, Q.; Wang, L. Cemented backfilling performance of yellow phosphorus slag. *Int. J. Miner., Metall. Mater.* **2010**, *17* (1), 121−126.
(61) Zhao, N.; Wang, S.; Quan, X.; Liu, K.; Xu, J.; Liu, B.; Liu, Y. Effects of Fly Ash and Bentonite on Mechanical and Durability Properties of Fiber Reinforced Geopolymer. *JOM* **2023**, *75* (3), 848−858.
(62) Gervais, C.; Ouki, S. K. Performance study of cementitious systems containing zeolite and silica fume: effects of four metal nitrates on the setting time, strength and leaching characteristics. *J. Hazard. Mater.* **2002**, *93* (2), 187−200.
(63) Wu, K.; Shi, H.; Xu, L.; Gao, Y.; Ye, G. Effect of Mineral Admixture on Mechanical Properties of Concrete by Adjusting Interfacial Transition Zone Microstructure. *J. Chin. Ceram. Soc.* **2017**, *45* (05), 623−630.
(64) Gupta, S.; Kua, H. W.; Pang, S. D. Effect of biochar on mechanical and permeability properties of concrete exposed to elevated temperature. *Constr. Build. Mater.* **2020**, *234*, 117338.
(65) Nazari, A.; Riahi, S. Microstructural, thermal, physical and mechanical behavior of the self compacting concrete containing SiO2 nanoparticles. *Mater. Sci. Eng., A* **2010**, *527* (29−30), 7663−7672.
(66) Bernal, J.; Reyes, E.; Massana, J.; León, N.; Sánchez, E. Fresh and mechanical behavior of a self-compacting concrete with additions of nano-silica, silica fume and ternary mixtures. *Constr. Build. Mater.* **2018**, *160*, 196−210.
(67) Zarnaghi, V. N.; Fouroghi-Asl, A.; Nourani, V.; Ma, H. On the pore structures of lightweight self-compacting concrete containing silica fume. *Constr. Build. Mater.* **2018**, *193*, 557−564.

https://doi.org/10.1021/acsomega.3c08560
ACS Omega 2024, 9, 1870−1880